

1 **Model aided quantification of dissolved carbon and** 2 **nitrogen release after windthrow disturbance in an Austrian** 3 **karst system**

4
5 **A. Hartmann^{1,2}, J. Kobler³, M. Kralik³, T. Dirnböck³, F. Humer³ and M. Weiler¹**

6 [1] Faculty of Environment and Natural Resources, Freiburg University, Germany

7 [2] Department of Civil Engineering, University of Bristol, UK

8 [3] Environment Agency Austria, Vienna, Austria

9 Correspondence to: A. Hartmann (andreas.hartmann@hydrology.uni-freiburg.de)

10 11 **Abstract**

12 Karst systems are important for drinking water supply. Future climate projections indicate
13 increasing temperature and a higher frequency of strong weather events. Both will influence
14 the availability and quality of water provided from karst regions. Forest disturbances such as
15 windthrow can disrupt ecosystem cycles and cause pronounced nutrient losses from the
16 ecosystems. In this study, we consider the time period before and after the wind disturbance
17 period (2007/08) to identify impacts on DIN (dissolved inorganic nitrogen) and DOC (dissolved
18 organic carbon) with a process-based flow and solute transport simulation model. Calibrated
19 and validated before the disturbance the model disregards the forest disturbance and its
20 consequences on DIN and DOC production and leaching. It can therefore be used as a base-line
21 for the undisturbed system and as a tool for the quantification of additional nutrient production.
22 Our results indicate that the forest disturbance by windthrow results in a significant increase of
23 DIN production lasting ~3.7 years and exceeding the pre-disturbance average by 2.7 kg/ha/a
24 corresponding to an increase of 53%. There were no significant changes of DOC
25 concentrations. With simulated transit time distributions we show that the impact on DIN
26 travels through the hydrological system within some months. But a small fraction of the system
27 outflow (<5%) exceeds mean transit times of >1 year.

28 **1 Introduction**

29 Karst systems contribute around 50% to Austria's drinking water supply (COST, 1995). Karst
30 develops due to the dissolvability of carbonate rock (Ford and Williams, 2007) and it results in
31 strong heterogeneity of subsurface flow and storage characteristics (Bakalowicz, 2005). The
32 resulting complex hydrological behavior requires adapted field investigation techniques
33 (Goldscheider and Drew, 2007). Future climate trajectories indicate increasing temperature
34 (Christensen et al., 2007) and a higher frequency of hydrological extremes (Dai, 2012;
35 Hirabayashi et al., 2013). Both will influence the availability and quality of water provided
36 from karst regions because temperature triggers numerous biogeochemical processes and fast
37 throughflow water has a disproportional effect upon water quality. Also forest disturbances
38 (windthrows, insect infestations, droughts) pose a threat on water quality through the
39 mobilization of potential pollutants and these disturbances are likely to increase in future
40 (Johnson et al., 2010; Seidl et al., 2014).

41 A way to quantify the impact of changes in climatic boundary conditions on the hydrological
42 cycle are simulation models. Special model structures have to be applied for karst regions to
43 account for their particular hydrological behavior (Hartmann et al., 2014a). A range of models
44 of varying complexity is available from the literature, that deal with the karstic heterogeneity,
45 such as groundwater flow in the rock fracture matrix and dissolution conduits (Jourde et al.,
46 2015; Kordilla et al., 2012), varying recharge areas (Hartmann et al., 2013a; Le Moine et al.,
47 2008) or preferential recharge by cracks in the soil or fractured rock outcrops (Rimmer and
48 Salingar, 2006; Tritz et al., 2011).

49 Nitrate and dissolved organic carbon (DOC) have both been considered in drinking water
50 directives and water preparation processes (Gough et al., 2014; Mikkelsen et al., 2013; Tissier
51 et al., 2013; Weishaar et al., 2003). Though nitrate pollution of drinking water is usually
52 attributed to fertilization of crops and grassland, an excess input of atmospheric nitrogen (N)
53 from industry, traffic and agriculture into forests has caused reasonable nitrate losses from
54 forest areas (Butterbach-Bahl et al., 2011; Erisman and Vries, 2000; Gundersen et al., 2006;
55 Kiese et al., 2011). The Northern Limestone Alps area is exposed to particularly high nitrogen
56 deposition (Rogora et al., 2006) and nitrate leaching occurs in increased rates (Jost et al., 2010).
57 Apart from this, forest disturbances such as windthrow and insect outbreaks disrupt the N cycle
58 and cause pronounced nitrate losses from the soils, at least in N saturated systems, that received
59 elevated N deposition due to elevated NO_x in the atmosphere (Bernal et al., 2012; Griffin et al.,

60 2011; Huber, 2005). Contrary to N deposition, atmospheric deposition of DOC is low (Lindroos
61 et al., 2008) and thus has not been identified as major driver of DOC leaching from subsoil
62 (Fröberg et al., 2007; Kaiser and Kalbitz, 2012; Verstraeten et al., 2014). Moreover, studies
63 show contrasting results but point to increased DOC (TOC) leaching from soil and catchments
64 after forest disturbances (Huber et al., 2004; Löfgren et al., 2014; Meyer et al., 1983; Mikkelsen
65 et al., 2013; Wu et al., 2014).

66 While many studies identify N and DOC as source of contamination in karst systems (Einsiedl
67 et al., 2005; Jost et al., 2010; Katz et al., 2001, 2004; Tissier et al., 2013) or provide static
68 vulnerability maps (Andreo et al., 2008; Doerfliger et al., 1999), only very few studies use
69 models to quantify the temporal behavior of a contamination through the systems (Butscher and
70 Huggenberger, 2008). Some studies use N and DOC to better understand karst processes
71 (Charlier et al., 2012; Mahler and Garner, 2009; Pinault et al., 2001) or for advanced karst
72 model calibration (Hartmann et al., 2013b, 2014b) but from our knowledge there are no
73 applications of such approaches to quantify the drainage processes of N and DOC, and
74 particularly so after strong impacts on ecosystems (e.g. windthrow) that release reasonable
75 amount of nitrate from the forest soils.

76 In this study, we consider the time period before and after storm Kyrill (early 2007) and several
77 other storm events (2008) that hit Middle Europe. The storms, from now on referred to as the
78 wind disturbance period, caused strong damage to the forests in our study area, a dolomite karst
79 system. We apply a new type of semi-distributed model that considers the spatial heterogeneity
80 of the karst system by distribution functions. We aimed at comparing the hydrological and
81 hydrochemical behavior (DOC, DIN) of the system before and during the wind disturbing
82 period. In particular, we wanted to understand if and how DOC and DIN input to the
83 hydrological system changed by the impact of the storms. Furthermore, we used virtual tracer
84 experiments to create transit time distributions that expressed how the impact of the storms
85 propagated through the variable dynamic flow paths of the karst system. This allowed us to
86 assess the vulnerability of the karst catchment to such impacts.

87 **2 Study site**

88 The study site LTER Zöbelboden is located in the northern part of the national park “Kalkalpen”
89 (Figure 1). Its altitude ranges from 550 m to 956 m ASL and its area is ~5.7 km². Mean monthly
90 temperature varies from -1 °C in January to 15.5 °C in August. The average temperature is 7.2
91 °C (at 900 m ASL). Annual precipitation ranges from 1,500 to 1,800 mm and snow accumulates

92 commonly between October and May with an average duration of about 4 months. The mean
93 N deposition in bulk precipitation between 1993 and 2006 was $18.7 \text{ kg N ha}^{-1} \cdot \text{yr}^{-1}$, out of which
94 15.3 kg N (82%) was inorganic (approximately half as NO_3^- -N and half as NH_4^+ -N) (Jost et al.,
95 2011). Due to the dominating dolomite, the catchment is not as heavily karstified as limestone
96 karst systems, but shows typical karst features such as conduits and sink holes (Jost et al., 2010).
97 The site can be split into steep slopes ($30\text{-}70^\circ$, 550-850 m ASL) and a plateau (850-950 m ASL),
98 with the plateau covering $\sim 0.6 \text{ km}^2$. Chromic cambisols and hydromorphic stagnosols with an
99 average thickness of 50 cm and lithic and rendzic leptosols with an average thickness of 12 cm
100 can be found at the plateau and the slopes, respectively (WRB, 2006). Both plateau and slopes
101 are mainly covered by forest. Norway spruce (*Picea abies* L. Karst.) interspersed with beech
102 (*Fagus sylvatica* L.) was planted after a clear cut around the year 1910. The vegetation at the
103 slopes is dominated by semi-natural mixed mountain forest with beech (*Fagus sylvatica*) as the
104 dominant species, Norway spruce (*P. abies*), maple (*Acer pseudoplatanus*), and ash (*Fraxinus*
105 *excelsior*). At the slopes no forest management has been conducted since the implementation
106 of the National Park.

107 **2.1 Available data**

108 A 10 year record of input and output observations was available. Starting from the hydrological
109 year 2002/03 it envelops well the stormy period that began in January 2007. It included daily
110 rainfall measurements and stream discharge measurements from stream sections 1 and 2 (Figure
111 1). We obtained the discharge of the entire system with a simple topography based up-scaling
112 procedure that is described in more detail in (Hartmann et al., 2012a). Irregular (weekly to
113 monthly) observations of DOC, DIN and SO_4^{2-} concentrations are available for precipitation
114 and at weir 1. DOC (entire study period), NO_3^- , SO_4^{2-} and NH_4^+ (since January 2010) samples
115 were filtered (MILLIPOR HTTP04700 ($0.4 \mu\text{m}$) (Millipor Corporation, USA)) with SM 16249
116 (Sartorius AG, Germany) (xxxx-2009) and SM 16201/19/20 (Sartorius AG, Germany) (2009-
117 xxxx). NH_4^+ concentrations were measured after filtering by spectrophotometry (Milton Roy
118 Spectronic 1201 (Thermo Fisher Scientific Inc., USA). Weekly DOC, SO_4^{2-} and NO_3^- samples
119 were pooled to provide volume weighted bi-weekly (until March 2009) and monthly
120 (thereafter) samples. DOC samples were acidified with 0.5 ml HCl 25%. All samples were kept
121 at 4°C until analyses. NO_3^- and SO_4^{2-} concentrations were determined by ion chromatography
122 with conductivity detection (Bulk precipitation: 2002-2009: Dionex ICS DX 500 (Dionex
123 Corp., USA); 2010-xxxx: Dionex ICS 3000 (Dionex Corp., USA); Runoff: 2001-2002: Dionex

124 ICS DX 500 (Dionex Corp., USA); 2002-2010: Metrohm ICS 7xx (Deutsche METROHM
125 GmbH & Co. KG, Germany)). DOC concentrations were measured with a Maihak Tocor 100
126 (SICK MAIHAK GmbH, Germany) (1996-2007) and a CPN TOC/DOC-Analyzer (Shimadzu
127 Corp., Japan) (2007-2010). DIN input was then calculated as the sum of NO_3^- -N and NH_4^+ -N.
128 Since NH_4^+ is either transformed into NO_3^- or absorbed in the soil NH_4^+ concentrations in runoff
129 are very small or not detectable. Therefore we calculated DIN outputs as NO_3^- -N. Additionally,
130 irregular observations of snow water equivalent at the plateau allowed for independent setup of
131 the snow routines.

132 **2.2 Recent disturbances**

133 Kyrill in the year 2007 and some similarly strong storms that followed 2008 caused some major
134 windthrows as well as single tree damages. A windthrow disturbance of ~ 5 ha occurred
135 upstream of weir 1. Though no direct measurements exist as to the total extent of the windthrow
136 area we estimate that 5-10 % of the study site has been subject to windthrow (Kobler et al.,
137 2015). We did not observe a significant change in intra- and inter-annual variability of DOC
138 concentrations and discharge before and during the wind disturbance period (Figure 2ae).
139 Runoff concentrations of DIN showed clear responses to the disturbances. With the first
140 windthrow event it started to increase until 2008/09 and slowly decreased again in 2010/11
141 (Figure 2c). Comparing DOC concentrations with discharge before and during the wind
142 disturbance period revealed a similar pattern. As shown by other studies on DOC mobilization
143 (e.g., Raymond and Saiers, 2010), a positive correlation between concentrations and discharge
144 (on log10 scale) occurred for DOC with concentrations up to 6 mg/l during high discharge
145 (similar to Frank et al., 2000). But there was no obvious difference between the pre-disturbance
146 period (Figure 2b).

147 **3 Methods**

148 **3.1 The model**

149 **3.1.1 Model hydrodynamics**

150 The semi-distributed simulation model considers the variability of karst system properties by
151 statistical distribution functions spread over $Z=15$ model compartments (Figure 3). That way it
152 simulates a range of variably dynamic pathways through the karst system. The detailed
153 equations of the model hydrodynamics are similar to its previous applications (Hartmann et al.,

154 2013a, 2013c, 2014b). They are described in the Appendix. Since in our case the model is used
 155 to simulate the discharge of the entire system and a weir within the system some small
 156 modifications had to be performed. Preceding studies showed that weir 1 (Figure 1) receives its
 157 discharge partially from the epikarst and partially from the groundwater, reaching it partially as
 158 concentrated and partially as diffuse flow (Hartmann et al., 2012a). Consequently we derive its
 159 discharge Q_{weir} [l/s] by

$$160 \quad Q_{weir}(t) = f_{Epi} \cdot \left[f_{Epi,conc} \cdot \sum_i^Z R_{conc,i}(t) + (1 - f_{Epi,conc}) \cdot \sum_i^Z R_{diff,i}(t) \right] +$$

$$\quad (1 - f_{Epi}) \cdot \left[f_{GW,conc} \cdot Q_{GW,Z}(t) + (1 - f_{GW,conc}) \cdot \sum_i^{Z-1} Q_{GW,i}(t) \right]$$

161 Where f_{Epi} is the fraction from the epikarst and $(1 - f_{Epi})$ the fraction from the groundwater. $f_{Epi,conc}$
 162 and $f_{GW,conc}$ represent the concentrated flow fractions of the epikarst and groundwater
 163 contributions, respectively. Table 1 lists all model parameters including a short description.

164 **3.1.2 Model solute transport**

165 To model the non-conservative transport of DOC and, DIN and SO_4^{2-} , we equipped the model
 166 with solute transport routines. SO_4^{2-} was included as an additional calibration variable because
 167 it proved to be important to reduce model equifinality (Beven, 2006) by adding additional
 168 information about groundwater dynamics (Hartmann et al., 2013a, 2013b). The inclusion of
 169 these 3 solutes allowed for a more reliable estimation of model parameters (Hartmann et al.,
 170 2012b, 2013a) and, further on, the evaluation of possible changes in the dynamic of solute
 171 concentrations during the stormy period. For most of the model compartments they simply
 172 followed the assumption of complete mixing. But to represent net production and leaching of
 173 DOC and DIN in the soil, as well as dissolution of SO_4^{2-} in the rock matrix, additional processes
 174 were included in the model structure. Similar to preceding studies (Hartmann et al., 2013a,
 175 2014b) SO_4^{2-} dissolution $G_{SO_4,i}$ [mg/l] for compartment i is calculated by:

$$176 \quad G_{SO_4,i} = G_{max,SO_4} \cdot \left(\frac{Z - i + 1}{Z} \right)^{a_{Geo}} \quad (2)$$

177 where a_{Geo} [-] is another variability parameter and G_{max,SO_4} [mg/l] is the equilibrium
 178 concentration of SO_4^{2-} in the matrix. DOC is mostly mobilised at in the forest floor (Borken et
 179 al., 2011). Stored in the soil or diffusively and slowly passing downwards, large parts of the
 180 DOC is absorbed or consumed by micro-organisms. But when lateral flow and concentrated

181 infiltration increase net leaching of DOC increases as well. For that reason our DOC transport
 182 routine only provides water to the epikarst when it is saturated (Eq. 10) with increasing DOC
 183 net production toward the more dynamic model compartments (Figure 3). Its DOC
 184 concentration $P_{DOC,i}$ [mg/l] for each model compartment is found by:

$$185 \quad P_{DOC,i} = P_{DOC} \cdot \left(\frac{Z-i+1}{Z} \right)^{-\frac{1}{a_{DOC}}} \quad (3)$$

186 where a_{DOC} [-] is the DOC variability constant and P_{DOC} [mg/l] is the DOC net production at
 187 soil compartment 1. Similar to other studies that assessed N input to a karst system (Pinault et
 188 al., 2001) we used a trigonometric series to assess the time variant net production of DIN, $P_{DIN,i}$
 189 [mg/l], to the soil:

$$190 \quad P_{DIN,i} = P_{DIN} + A_{DIN} \cdot \sin\left(\frac{365.25}{2\pi} \cdot (J_D + S_{PH,DIN})\right) \quad (4)$$

191 Here, P_{DIN} is the mean amount of dissolved inorganic N in the soil solution, while A_N [mg/l]
 192 and $S_{PH,DIN}$ [d] are the amplitude of the seasonal signal and the phase shift of seasonal DIN
 193 uptake (immobilisation by plants and soil organisms) and release (net DIN in the soil water)
 194 cycle, respectively. J_D is the Julian day of each calendar year. Due to its seasonal variation $P_{DIN,i}$
 195 can also be negative meaning that uptake of DIN takes place.

196 **3.2 Model calibration and evaluation**

197 With 14 model parameter that controlled the hydrodynamics and 7 parameters that allow for
 198 the non-conservative solute transport, the calibration of the model was a high-dimensional
 199 problem. For that reason we have chosen the Shuffled Complex Evolution Metropolis algorithm
 200 SCEM (Vrugt et al., 2003) that prove itself to be capable of exploring high dimensional
 201 optimization problems (Fenicia et al., 2014; Feyen et al., 2007; Vrugt et al., 2006). As
 202 performance measure we used the Kling-Gupta efficiency KGE (Gupta et al., 2009). For
 203 calibration, KGE was weighted equally among all solutes, 1/3 for the discharge of the entire
 204 system, and 2/3 for the discharge of weir 1 whose observations precision was regarded to be
 205 more reliable than the up-scaled discharge. KGE is defined as:

$$206 \quad KGE = 1 - \sqrt{(r-1)^2 + (\alpha-1)^2 + (\beta-1)^2} \quad (5)$$

207
$$\text{with } \alpha = \frac{\sigma_s}{\sigma_o} \text{ and } \beta = \frac{\mu_s}{\mu_o} \tag{6}$$

208 where r is the linear correlation coefficient between simulations and observations, μ_s/μ_o and
209 σ_s/σ_o are the means and standard deviations of simulations and observations, respectively. α
210 expresses the variability and β the bias.

211 To check for the stability of the calibrated parameters, we perform a split-sample test (Klemeš,
212 1986). Since the pre-disturbance time series was too short to be split into two equally long
213 periods, we perform a both-sided split-sample test by bootstrapping two independent 4-year
214 time series of observations (1st sample: discrete sampling of 50% of the values of each observed
215 time series, 2nd sample: remaining 50% of the observations). We calibrate our model with the
216 1st sample and evaluate it with the 2nd sample, and vice versa. A parameter set is regarded stable,
217 when the calibration with both samples yields similar parameter sets and their KGE concerning
218 discharge and the solutes does not reduce significantly when applying them on the other sample.

219 **3.3 Change of hydrochemical behaviour with the stormy period**

220 After the model evaluation, we use the different components of the KGE in Eqs. (5) and (6) to
221 explore the impacts of the storm disturbance period on the hydrochemical components.
222 Assuming that the model is able to predict to hydrochemical behaviour that prevailed without
223 the impact of the storms adapting the hydrochemical parameters of the model in Eqs. (3)-(4)
224 and analysing the difference between the adapted hydrochemical simulations and the non-
225 adapted simulations will allow us to quantify the change of solute mass balance due to the storm
226 impact. We define the time span for our adaption as the time when the different components of
227 KGE exceed the range of their pre-disturbance variability. During this time period we
228 compensate for the apparent deviations by adapting the hydrochemical parameters. This is done
229 twice, once by manual adaption and another time using an automatic calibration scheme. Their
230 new values will indicate changes of the seasonality, production or inter-annual variations.

231 **3.4 Transit time distributions**

232 The signal of the storm impact will travel by various velocities and pathways through the karst
233 system. While fast flow paths and small storages will transport the signal rapidly to the system
234 outlet, slow pathways and large storages will delay and dilute the signal. Transit time
235 distributions indicate how fast surface impacts travel through the hydrological system. We

236 derive transit time distributions from the model by performing a virtual tracer experiment with
237 continuous injection over the entire catchment at the beginning of the impact of the stormy
238 period. When a model compartment reaches 50% of the tracer concentration is considered as
239 median transit time. The hereby-derived transit times will elaborate how the hydrological
240 system propagates the signal through the system including all slow and fast pathways as defined
241 by Eqs. (12) and (18). As for DIN and DOC we assume complete and instantaneous mixing
242 with each model storage (soil, epikarst, and groundwater) at each compartment, the time that
243 we refer to as “mean transit time” of a model compartment is the time the virtual tracer needs
244 to pass through the particular model storage. In combination with the fluxes that are provided
245 from each of the model compartments, it is possible to quantify the fractional contribution of
246 fast and slow flow paths, respectively. We will apply the virtual tracer from the previously
247 assessed beginning of the impact until the end of the time series to assess the transit time
248 distribution. In addition, we apply a second virtual tracer that also lasts only for the disturbance
249 period (as estimated in subsection 3.3) to evaluate the filter and retardation potential of the karst
250 system.

251 **4 Results**

252 **4.1 Model performance**

253 Table 1 shows the calibrated parameters for the two samples. They indicate a thick soil and a
254 relatively thin epikarst. The dynamics expressed by the storage constants indicate days and
255 weeks for the conduits (model compartment $i=Z$) and the epikarst, respectively. The distribution
256 coefficient of the groundwater is larger than the soil/epikarst storage constant. For DOC and
257 DIN there are a natural production rates of 1.6-1.8 mg/l and -1.35-0.1 mg/l, respectively. The
258 DOC distribution coefficient is between 0.9 and 1.1. The phase shift and amplitude for DIN
259 showed that there is a seasonal variation of DIN net production with its maximum release at
260 April each year for both of the samples. SO_4^{2-} is dominated by the concentration in the
261 precipitation input with some leaching in the soil and sulphides in the dolomite. Its variability
262 constant is quite low (<0.1). Weighted KGEs, as well as their values for the individual
263 simulation variables are relatively stable. Overall, calibration on both samples provided similar
264 parameter values. Due to its higher stability concerning the evaluation period, we chose the 2nd
265 sample for further analysis.

266 The discharge simulations follow adequately the variations of the observations (Figure 4),
267 although some small events are not reproduced by the model and although the simulations of
268 the weir's discharge tend to under-estimate peak flows. No obvious differences can be seen
269 between the pre-disturbance and wind disturbance period. The hydrochemical simulations tend
270 to follow the observations, as well (Figure 5). But there is sometimes some under-estimation of
271 the DOC peaks for the pre-disturbance period. The DIN simulations appear to be more precise
272 during the pre-disturbance period but there is a systematic under-estimation when the
273 disturbance takes place.

274 **4.2 Model performance during the wind disturbance period**

275 There is a deviation between pre-disturbance and disturbance period simulated and observed
276 variability and bias for DIN (Figure 6). A similar tendency can be found for DOC. But only for
277 DIN the deviations are different to the variations already found during the pre-disturbance
278 period (which is also the calibration/validation period). The variations of DOC appear to be
279 systematic, too, but they fall within its ranges of variability during the pre-disturbance period.

280 **4.3 Adaption of N parameters for the wind disturbance period**

281 The very first signs of the impact were found at May 1st 2007 lasting to the end of the
282 hydrological year 2010/11. In a first trial (Table 2), the model parameters for the DIN
283 production were adapted manually to compensate for the changes of observed DIN
284 concentrations with focus on reducing the difference indicated by the bias β and variability α
285 components of the KGE_{DIN} . In a second trial, we use an automatic calibration scheme to achieve
286 the optimum KGE_{DIN} . As indicated by the highest KGE (Table 2), the automatic calibration
287 provided the highest KGE_{DIN} . But this is achieved by improving variability α and correlation r .
288 Almost no improvement is reached for the bias β . Even though resulting in a slightly lower
289 improvement of KGE_{DIN} the manual calibration results in a much more acceptable reduction of
290 the bias (Figure 6). Its parameter values showed a production rate P_{DIN} of DIN more than two
291 times 2 mg/l than the pre-disturbance value, an amplitude A_{DIN} more than 4 times larger, and a
292 phase shift $S_{PH,DIN}$ towards a week earlier in the year, resulting in a more acceptable simulation
293 of DIN dynamics during the disturbance period (Figure 7).

294 **4.4 Transit time distributions**

295 The transit time distributions show that the soil and epikarst system reacts quite rapidly to the
296 virtual injection. 50% of the injection concentration is reached within ~60 days (Figure 8a),
297 while most of groundwater system requires ~100 days to reach 50% of the injection
298 concentration with few flow paths reach up to 300 days (Figure 8c). A similar behaviour is
299 found when the impact ends (Figure 8bd). It also shows that some of the slowest flow paths just
300 reach the input concentration before they start to decline again.

301 **5 Discussion**

302 **5.1 Reliability of calibrated parameters and model simulations**

303 Most of the calibrated model parameters are in ranges that are in accordance with other
304 modelling studies or field evidence. General differences between the calibrated parameter
305 values of the both-sided split sample test may mostly be due to the comparatively low resolution
306 of the hydrochemical variables (SO₄, DOC and DIN) that even increased by the bootstrapping
307 procedure. However, the good multi-objective simulation performance of the model, as well as
308 its evaluation by the split sample test an overall acceptable performance of the model. With
309 almost 3-8 days the epikarst storage constant is in accordance with field studies on the epikarst
310 storage behaviour that found retention times of some days to few weeks (Aquilina et al., 2006;
311 Perrin et al., 2003). The soil as well as the epikarst storage capacity are quite large. These high
312 values may be explained by structural errors of the model that result in unrealistic calibrated
313 parameter values, in particular possible parameter interactions between their storage capacities
314 and storage coefficients. Since the soil and the vegetation controls the fraction of rain that is
315 lost to evapotranspiration this high calibrated value might be due to tree roots ranging through
316 the soil into the epikarst (Heilman et al., 2012) or rock debris (Hartmann et al., 2012a).

317 Similar to the epikarst storage constant, the conduit storage constant, K_C , is, with its value of
318 1.1 days, in the range of previous modelling studies (Fleury et al., 2007; Hartmann et al.,
319 2013a). The high values of the epikarst variability constant and the groundwater constant
320 indicate a low development of preferential flow paths in the rock, which is typical for dolomite
321 aquifers (Ford and Williams, 2007). A low degree of karstification was already known for our
322 study site (Jost et al., 2010) and the calibrated recharge areas fall well into the ranges found in
323 previous modelling studies (Hartmann et al., 2012a, 2013c).

324 The hydrochemical parameters mostly show realistic values. A DOC production parameter
325 P_{DOC} of ~1.6-1.8 mg/l resulted in realistic simulated concentrations at the weir. For DIN
326 production the two calibration samples result in values of -1.4 and 0.1 mg/l, going along with
327 amplitudes of 3.4 and 1.8, respectively. Hence, there appears to be some correlation between
328 the production and amplitude parameters, P_{DIN} and A_{DIN} . Negative values indicate that during
329 some periods of the year all DIN is consumed by plants or soil organisms and that the production
330 period is shorter, but more pronounced due to its larger value of amplitude. But we expect these
331 differences to be minor since the phase shift $S_{PH,DIN}$ of both calibration samples is almost the
332 same, as well as their annual maximum ($P_{DIN} + A_{DIN}$) of 2.01 mg/l and 1.95 mg/l. It indicates a
333 maximum of DIN production and leaching at the time of the year when snow melt reaches its
334 maximum (March to April) and when DIN uptake by plants is still low (Jost et al., 2010). The
335 dissolution equilibrium concentrations of 2.7-3.1 mg/l for SO_4^{2-} indicate the abundance of the
336 precipitation-input, oxidation of sulphides (e.g. pyrite) in the dolomite and traces of evaporates
337 in the small Plattenkalk occurrences (Kralik et al., 2006).

338 **5.2 Impact of storms**

339 The deviation between simulated and observed time series (Figure 5) already indicates that DIN
340 is the only solute that shows a clear impact of the storms. This is further corroborated by
341 considering the individual components of KGE in Figure 6. It is well known that nitrate leaching
342 to the groundwater increases sharply after tree damage (dieback) in forests where N is not
343 strongly limited (Bernal et al., 2012; Griffin et al., 2011; Huber, 2005). Such disturbances
344 disrupt the N cycle. The loss of tree N uptake favours nitrification of surplus NH_4^+ by
345 microorganism. Moreover, above- (i.e. foliage) and belowground (i.e. fine roots) litter from
346 dead trees enhances the mineralization of organic matter, ammonification and nitrification.
347 Both processes are accelerated by increased soil moisture and soil temperature due to the loss
348 of the forest canopy. Subsequently, leaching of N increases with increased seepage fluxes due
349 to decreased interception and water uptake by trees. Since the simple DIN routine of the model
350 cannot take into account such changes the under-estimated DIN concentrations and their
351 amplitude show the effect of forest disturbance on the leaching of DIN from the studied
352 catchment. There is also an apparently systematic deviation of the DOC variability α . But its
353 variations during the pre-storm period are similarly large and thus points to a negligible effect
354 of forest disturbance on DOC leaching. Numerous studies identified the forest floor as DOC
355 source (Borken et al., 2011; Michalzik et al., 2001). Windthrow generally causes a (short-term)

356 pulse of above- and belowground litter (Harmon et al., 2011). Thereby, mineralization of the
357 surplus litter input concurrent with improved soil climatic conditions likely increased the
358 leaching of DOC from the forest floor (Fröberg et al., 2007; Kalbitz et al., 2007). Concurrent,
359 increased soil water, surface and shallow subsurface flow may favour increased soil DOC
360 leaching to downslope surface waters (Monteith et al., 2006; Neff and Asner, 2001; Sanderman
361 et al., 2009). In mountainous catchment the latter flow paths are likely due to the steepness of
362 the catchment slopes (Boyer et al., 1997; Sakamoto et al., 1999; Terajima and Moriizumi,
363 2013). The missing signal of forest disturbance on DOC concentrations at the weir 1 even
364 shortly after the disturbance may be due to the minor extension of the disturbed area, the minor
365 increase of surface and shallow subsurface flow due to the relative low slope of the disturbed
366 area, the buffering of increased topsoil DOC leaching due to absorption of DOC within the
367 subsoil (Borken et al., 2011; Huber et al., 2004), missing DOC-rich riparian source areas (i.e.
368 wetlands, floodplains) and the reduction pre-disturbance organic matter input to soil (i.e. litter,
369 root exudates) (Högberg and Högberg, 2002). Theoretically, hydrological processes such as a
370 decrease of transpiration or an increase of groundwater recharge may also occur. But these
371 superficial changes are probably minor considering the typically high karstic infiltration
372 capacities that remove surface water quite rapidly (Hartmann et al., 2014b, 2015). For both,
373 disturbance induced changes of DOC and hydrological processes, more sampling in high
374 temporal-resolution should be undertaken to elucidate the effect of forest disturbance within
375 the studied ecosystem.

376 **5.2.1 N leaching from the soil**

377 Adapting the DIN solute transport parameters by an automatic calibration scheme resulted in
378 an increased KGE_{DIN} (Figure 7). But it did not resolve the bias of simulated and observed DIN
379 concentrations during the wind disturbance period since the overall improvement of KGE_{DIN}
380 was reached by an improvement of r and α (Table 2). Adjusting the DIN parameters manually
381 resulted in a more acceptable decrease of the bias β that also went along with an increase of the
382 overall KGE_{DIN} . An increase of the DIN production rate of ~ 2 mg/l indicates a massive
383 mobilisation of DIN and a reduction of its seasonal amplitude by ~ 1.1 mg/l. Even though there
384 may be some correlation between mean annual production and amplitude (see previous section),
385 the annual maximum of 2.80 mg/l ($P_{DIN} + A_{DIN}$) indicates an increase of the DIN concentrations
386 in the soil of at least ~ 0.8 mg/l (from 1.95 to 2.01 mg/l at the pre-disturbance period).

387 We identified the beginning of the impact at May 1st 2007 and its end by the end of the
388 hydrological year 2010/11. This is more than 2 years after the last storm in 2008 indicates how
389 long the ecosystem takes to recover from the disturbance. Other studies have shown comparable
390 recovery times (Katzensteiner, 2003; Weis et al., 2006) or longer (Huber, 2005). Considering
391 the deviations between DIN simulations by the pre-disturbance calibration and the DIN
392 simulations obtained by the manual adjustment, they sum up to an additional release of 9.9
393 kg/ha of DIN over the whole period of ~3.7 years, or 2.7 kg/ha/a in addition to 5.8 kg/ha/a that
394 would have been released without the wind disturbance. These values only corresponds to
395 inorganic N. Other studies showed that also dissolved organic N can contribute to vertical
396 percolation but only in small ratios from 2-5% (Solinger et al., 2001; Wu et al., 2009). The
397 apparent shift of $S_{PH,DIN}$ towards an earlier maximum of DIN release (7 days) may probably be
398 due to the earlier onset of snow melt in open areas as compared to forests because snow melt is
399 a major driver of DIN leaching from the soils in our study area (Jost et al., 2010).

400 **5.2.2 N propagation through the hydrological system**

401 The virtual tracer injections that we applied with the beginning of the disturbance period
402 elaborate the hydrological system's filter and retardation capacity. Due to their higher dynamics
403 the soil and the epikarst system adapt more rapidly to the change within weeks and months.
404 Similar behaviour was also found in previous studies (Hartmann et al., 2012a; Kralik et al.,
405 2009). The majority of the simulated flow paths adapts to the virtual tracer signal within a few
406 months, which is in accordance with water isotope studies as the weir (Humer and Kralik, 2008;
407 Kralik et al., 2009). However, using age dating (CFC and SF6) and artificial tracer experiments
408 at individual springs within the study area, the Kralik et al. (2009) also found ages from several
409 days to several decades. Hence, the majority of transit times found by the virtual tracer
410 experiment reflect the average behaviour of the sub-catchment drained by the weir, which can
411 be regarded as more dominant than observations at individual the springs that rather represent
412 fast and slow flow paths of minor importance. The retardation is also visible from the dynamics
413 of the DIN concentrations just after the end of the disturbance period (beginning of 2011/12,
414 Figure 7). Even though DIN production is set to pre-disturbance conditions, it almost takes 4
415 months for the DIN simulations (by manual calibration) to adopt to their undisturbed
416 concentrations (pre-disturbance calibration). Due to their small contribution (<5%), the slower
417 flow paths do not have a significant impact on the retardation capacity of the hydrological
418 system.

419 **5.3 Implications**

420 Our results corroborate findings from many other studies that extreme events as during the wind
421 disturbance period in our study can result in significant increase of DIN in the runoff, despite
422 the area impacted was relative small (5-10% of the watershed). Particularly in karst catchments
423 such changes can happen quickly and prevail for a significant duration, in our case more than
424 2 years after the last storm. Due to subsurface heterogeneity the impact did not travel uniformly
425 through the system. It rather split into different pathways and mixed with old water that
426 percolated prior to the impact. In our system, large parts of the water travelled rapidly through
427 the system. But a smaller number of pathways had large storages of old water and slow flow
428 velocities resulting in significant retardation. Taking into account that forest disturbances will
429 most probably increase with climate change (Seidl et al., 2014), DIN mobilisation as observed
430 in our study may occur more often and more intense. The hydrological system may dilute and
431 delay rapid shifts of N concentration, and it will “memorize” the impacts for some time. But
432 our present analysis showed that the time scale of the wind disturbance on DIN production and
433 leaching from the soil exceeds the time scale of transit of the disturbance through the system.
434 This is most probably due to the small size and the subsurface karstic behaviour of our study
435 site that favours faster flow paths and low system storage than hydrological systems with larger
436 extent or with other types of geology.

437 **6 Conclusions**

438 In our study we used a process-based semi distributed karst model to simulate DOC, DIN and
439 SO_4^{2-} transport through a dolomite karst system in Austria. We calibrated and validated our
440 model during a 4-year time period just before a series of heavy storms caused strong wind
441 disturbance to the study site’ ecosystem. To quantify its impact we run the model for the entire
442 disturbance period using the parameters we found at the pre-storm period. The deviations
443 between the simulations and the observations gave us indication that there was a significant
444 shift in DIN mobilisation, its seasonal amplitude and its timing. Estimating the beginning and
445 end of the disturbance period we applied a continuous virtual tracer injection to obtain the mean
446 transit times of the karst system. They showed us how the hydrological system filtered and
447 retarded the impact of the disturbance at the system outlet.

448 Even though our study is only considering one site and one wind disturbance period it already
449 provides some generally applicable conclusions: (1) hydroclimatic extremes such as storms do
450 not only create droughts or floods; they can also affect water quality; (2) a hydrological system

451 can filter and delay surface impacts but it may also memorize past impacts but only at a limited
 452 time scale; (3) water quality models that have been calibrated without consideration of such
 453 external impacts will provide poor predictions. For these reasons we believe that future large-
 454 scale simulations of water resources have to include water quality simulations that take into
 455 account the impact of ecosystem disturbances. Even without anthropogenic contamination
 456 climate change will strongly affect water quality in our aquifers and streams and we have to
 457 understand and prepare ourselves to avoid threads on future water supply.

458 **7 Acknowledgements**

459 Financial support by the Transnational Access to Research Infrastructures activity in the 7th
 460 Framework Programme of the EC under the ExpeER project and the South East Europe
 461 Transnational Cooperation Programme OrientGate for conducting the research is gratefully
 462 acknowledged. This work was supported by a fellowship within the Postdoc Programme of the
 463 German Academic Exchange Service (DAAD).

464 **8 Appendix**

465 The variability of soil depths in the model is expressed by a mean soil depth $V_{mean,S}$ [mm] and
 466 a distribution coefficient a_{SE} [-]. The soil storage capacity $V_{S,i}$ [mm] for every compartment i is
 467 calculated by:

$$468 \quad V_{S,i} = (1 - f_{var,S}) \cdot V_{mean,S} + V_{max,S} \cdot \left(\frac{i}{Z}\right)^{a_{SE}} \quad (7)$$

469 Where the maximum soil storage capacity $V_{max,S}$ [mm] is derived from ($f_{var,S} \cdot V_{mean,S}$) as
 470 described in Hartmann et al. (2013c). $f_{var,S}$ [-] is the fraction of the soil that shows variable
 471 thicknesses while $(1 - f_{var,S})$ has uniform value. The same distribution coefficient a_{SE} is used to
 472 define the epikarst storage distribution by the mean epikarst depth $V_{mean,E}$ [mm] (derivation of
 473 $V_{max,E}$ identical to $V_{mean,S}$):

$$474 \quad V_{E,i} = V_{max,E} \cdot \left(\frac{i}{Z}\right)^{a_{SE}} \quad (8)$$

475 Actual evapotranspiration from each soil compartment at time step t $E_{act,i}$ is found by:

$$476 \quad E_{act,i}(t) = E_{pot}(t) \cdot \frac{\min[V_{Soil,i}(t) + P(t) + Q_{Surfacei}(t), V_{S,i}]}{V_{S,i}} \quad (9)$$

477 where $Q_{surface,i}$ [mm/d] is the surface inflow originating from compartment $i-1$ (see Eq. (13)),
 478 E_{pot} [mm/d] the potential evaporation, and P [mm/d] the precipitation at time t . E_{pot} is calculated
 479 by the Penman-Wendling approach (Wendling et al., 1991;DVWK, 1996). To account for the
 480 solid fraction of precipitation a snowmelt routine was set on top of the model. We used the
 481 same routine that was applied on 148 other catchments in Austria by Parajka et al. (2007) and
 482 explained in Hartmann et al. (2012). Recharge to the epikarst $R_{Epi,i}$ [mm/d] is defined as:

$$483 \quad R_{Epi,i}(t) = \max[V_{Soil,i}(t) + P(t) + Q_{Surface,i}(t) - E_{act,i}(t) - V_{S,i}, 0] \quad (10)$$

484 Where the storage coefficients $K_{E,i}$ [d] control the outflow of the epikarst:

$$485 \quad Q_{Epi,i}(t) = \frac{\min[V_{Epi,i}(t) + R_{Epi,i}(t) + Q_{Surface,i}(t), V_{E,i}]}{K_{E,i}} \cdot \Delta t \quad (11)$$

$$486 \quad K_{E,i} = K_{max,E} \cdot \left(\frac{Z - i + 1}{Z} \right)^{a_{SE}} \quad (12)$$

487 $K_{max,E}$ is derived by a mean epikarst storage coefficient $K_{mean,E}$ (see Hartmann et al., 2013c).
 488 Excess water from the soil and epikarst that produces surface flow to the next model
 489 compartment $Q_{Surf,i+1}$ [mm/d] is calculated by:

$$490 \quad Q_{Surf,i+1}(t) = \max[V_{Epi,i}(t) + R_{Epi,i}(t) - V_{E,i}, 0] \quad (13)$$

491 The lower outflow of each epikarst compartment is separated into diffuse ($R_{diff,i}$ [mm/d]) and
 492 concentrated groundwater recharge ($R_{conc,i}$ [mm/d]) by the recharge separation factor $f_{C,i}$ [-]:

$$493 \quad R_{conc,i}(t) = f_{C,i} \cdot Q_{Epi,i}(t) \quad (14)$$

$$494 \quad R_{diff,i}(t) = (1 - f_{C,i}) \cdot Q_{Epi,i}(t) \quad (15)$$

495 The distribution of $f_{C,i}$ among the different compartments is defined by the distribution
 496 coefficient a_{fsep} :

$$497 \quad f_{C,i} = \left(\frac{i}{Z} \right)^{a_{fsep}} \quad (16)$$

498 Diffuse recharge reaches the groundwater compartment below, while concentrated recharge is
 499 routed to the conduit system (compartment $i = Z$). The variable contributions of the
 500 groundwater compartments that represent diffuse flow through the matrix ($1 \dots Z - 1$) are given
 501 by

502
$$Q_{GW,i}(t) = \frac{V_{GW,i}(t) + R_{diff,i}(t)}{K_{GW,i}} \quad (17)$$

503 $K_{GW,i}$ is calculated by:

504
$$K_{GW,i} = K_C \cdot \left(\frac{Z-i+1}{Z} \right)^{-a_{GW}} \quad (18)$$

505 where K_C is the conduit storage coefficient. The groundwater contribution of the conduit system
506 originates from compartment Z :

507
$$Q_{GW,Z}(t) = \frac{\min \left[V_{GW,Z}(t) + \sum_{i=1}^Z R_{conc,i}(t), V_{crit,OF} \right]}{K_C} \quad (19)$$

508 Knowing the recharge area A_{max} [km²] and rescaling the dimensions [l s⁻¹], the discharge of the
509 entire system Q [l s⁻¹] is calculated by:

510
$$Q(t) = \frac{A_{max}}{Z} \cdot \sum_{i=1}^Z Q_{GW,i}(t) \quad (20)$$

511

512 9 References

513 Andreo, B., Ravbar, N. and Vías, J. M.: Source vulnerability mapping in carbonate (karst)
514 aquifers by extension of the COP method: application to pilot sites, *Hydrogeol. J.*, 17(3), 749–
515 758, doi:10.1007/s10040-008-0391-1, 2008.

516 Aquilina, L., Ladouche, B. and Doerfliger, N.: Water storage and transfer in the epikarst of
517 karstic systems during high flow periods, *J. Hydrol.*, 327, 472–485, 2006.

518 Bakalowicz, M.: Karst groundwater: a challenge for new resources, *Hydrogeol. J.*, 13, 148–
519 160, 2005.

520 Bernal, S., Hedin, L. O., Likens, G. E., Gerber, S. and Buso, D. C.: Complex response of the
521 forest nitrogen cycle to climate change, , doi:10.1073/pnas.1121448109/-
522 /DCSupplemental.www.pnas.org/cgi/doi/10.1073/pnas.1121448109, 2012.

523 Beven, K. J.: A manifesto for the equifinality thesis, *J. Hydrol.*, 320(1-2), 18–36 [online]
524 Available from: [http://www.sciencedirect.com/science/article/B6V6C-4H16S4M-](http://www.sciencedirect.com/science/article/B6V6C-4H16S4M-1/2/571c8821621c803522cc823147bef169)
525 [1/2/571c8821621c803522cc823147bef169](http://www.sciencedirect.com/science/article/B6V6C-4H16S4M-1/2/571c8821621c803522cc823147bef169), 2006.

526 Borken, W., Ahrens, B., Schulz, C. and Zimmermann, L.: Site-to-site variability and temporal
527 trends of DOC concentrations and fluxes in temperate forest soils, *Glob. Chang. Biol.*, 17(7),

528 2428–2443, doi:10.1111/j.1365-2486.2011.02390.x, 2011.

529 Boyer, E. W., Hornberger, G. M., Bencala, K. E. and McKnight, D. M.: Response
530 characteristics of DOC flushing in an alpine catchment, *Hydrol. Process.*, 11(12), 1635–1647,
531 doi:10.1002/(SICI)1099-1085(19971015)11:12<1635::AID-HYP494>3.0.CO;2-H, 1997.

532 Butscher, C. and Huggenberger, P.: Intrinsic vulnerability assessment in karst areas: A
533 numerical modeling approach, *Water Resour. Res.*, 44, W03408, doi:10.1029/2007WR006277,
534 2008.

535 Butterbach-Bahl, K., Gundersen, P., Ambus, P., Augustin, J., Beier, C., Boeckx, P.,
536 Dannenmann, M., Sanchez Gimeno, B., Ibrom, A. and Kiese, R.: Nitrogen processes in
537 terrestrial ecosystems, *Eur. nitrogen Assess. sources, Eff. policy Perspect.*, 99–125, 2011.

538 Charlier, J.-B., Bertrand, C. and Mudry, J.: Conceptual hydrogeological model of flow and
539 transport of dissolved organic carbon in a small Jura karst system, *J. Hydrol.*, 460-461, 52–64,
540 doi:10.1016/j.jhydrol.2012.06.043, 2012.

541 Christensen, J. H., Hewitson, B., Busuioc, A., Chen, A., Gao, X., Held, I., Jones, R., Kolli, R.
542 K., Kwon, W.-T., Laprise, R., Rueda, V. M., Mearns, L., Menéndez, C. G., Räisänen, J., Rinke,
543 A., Sarr, A. and Whetton, P.: Regional Climate Projections, in *Climate Change 2007: The
544 Physical Science Basis. Contribution of Working Group I to the Fourth Assessment Report of
545 the Intergovernmental Panel on Climate Change*, edited by S. Solomon, D. Qin, M. Manning,
546 Z. Chen, M. Marquis, K. B. Averyt, M. Tignor, and H. L. Miller, p. 996, Cambridge University
547 Press, Cambridge, United Kingdom and New York, NY, USA. [online] Available from:
548 [http://www.ipcc.ch/publications_and_data/publications_ipcc_fourth_assessment_report_wg1_](http://www.ipcc.ch/publications_and_data/publications_ipcc_fourth_assessment_report_wg1_report_the_physical_science_basis.htm)
549 [report_the_physical_science_basis.htm](http://www.ipcc.ch/publications_and_data/publications_ipcc_fourth_assessment_report_wg1_report_the_physical_science_basis.htm), 2007.

550 COST: COST 65: Hydrogeological aspects of groundwater protection in karstic areas, Final
551 report (COST action 65), edited by D.-G. X. I. I. S. European Commission Research and
552 Development, *Eur. Comm. Dir. XII Sci. Res. Dev.*, Report EUR, 446, 1995.

553 Dai, A.: Increasing drought under global warming in observations and models, *Nat. Clim.*
554 *Chang.*, 3(1), 52–58, doi:10.1038/nclimate1633, 2012.

555 Doerfliger, N., Jeannin, P.-Y. and Zwahlen, F.: Water vulnerability assessment in karst
556 environments: a new method of defining protection areas using a multi-attribute approach and
557 GIS tools (EPIK method), *Environ. Geol.*, 39(2), 165–176, 1999.

558 Einsiedl, F., Maloszewski, P. and Stichler, W.: Estimation of denitrification potential in a karst
559 aquifer using the ¹⁵N and ¹⁸O isotopes of NO₃⁻, *Biogeochemistry*, 72(1), 67–86 [online]
560 Available from: <http://dx.doi.org/10.1007/s10533-004-0375-8>, 2005.

561 Erisman, J. W. and Vries, W. de: Nitrogen deposition and effects on European forests, *Environ.*
562 *Rev.*, 8(2), 65–93, doi:10.1139/a00-006, 2000.

563 Fenicia, F., Kavetski, D., Savenije, H. H. G., Clark, M. P., Schoups, G., Pfister, L. and Freer,

564 J.: Catchment properties, function, and conceptual model representation: is there a
565 correspondence?, *Hydrol. Process.*, 28, 2451–2467, doi:10.1002/hyp.9726, 2014.

566 Feyen, L., Vrugt, J. a., Nualláin, B. Ó., van der Knijff, J. and De Roo, A.: Parameter
567 optimisation and uncertainty assessment for large-scale streamflow simulation with the
568 LISFLOOD model, *J. Hydrol.*, 332(3-4), 276–289, doi:10.1016/j.jhydrol.2006.07.004, 2007.

569 Fleury, P., Plagnes, V. and Bakalowicz, M.: Modelling of the functioning of karst aquifers with
570 a reservoir model: Application to Fontaine de Vaucluse (South of France), *J. Hydrol.*, 345, 38–
571 49, 2007.

572 Ford, D. C. and Williams, P. W.: *Karst Hydrogeology and Geomorphology*, Wiley, Chichester.,
573 2007.

574 Fröberg, M., Jardine, P. M., Hanson, P. J., Swanston, C. W., Todd, D. E., Tarver, J. R. and
575 Garten, C. T.: Low Dissolved Organic Carbon Input from Fresh Litter to Deep Mineral Soils,
576 *Soil Sci. Soc. Am. J.*, 71(2), 347, doi:10.2136/sssaj2006.0188, 2007.

577 Goldscheider, N. and Drew, D.: *Methods in Karst Hydrogeology*, edited by I. A. of
578 Hydrogeologists, Taylor & Francis Group, Leiden, NL., 2007.

579 Gough, R., Holliman, P. J., Heard, T. R. and Freeman, C.: Dissolved organic carbon and
580 trihalomethane formation potential removal during coagulation of a typical UK upland water
581 with alum, PAX-18 and PIX-322, *J. Water Supply Res. Technol.*, 63(8), 650–660, 2014.

582 Griffin, J. M., Turner, M. G. and Simard, M.: Nitrogen cycling following mountain pine beetle
583 disturbance in lodgepole pine forests of Greater Yellowstone, *For. Ecol. Manage.*, 261(6),
584 1077–1089, doi:10.1016/j.foreco.2010.12.031, 2011.

585 Gundersen, P., Schmidt, I. K. and Raulund-Rasmussen, K.: Leaching of nitrate from temperate
586 forests – effects of air pollution and forest management, *Environ. Rev.*, 14(1), 1–57,
587 doi:10.1139/a05-015, 2006.

588 Gupta, H. V, Kling, H., Yilmaz, K. K. and Martinez, G. F.: Decomposition of the mean squared
589 error and NSE performance criteria: Implications for improving hydrological modelling, *J.*
590 *Hydrol.*, 377(1-2), 80–91, doi:10.1016/j.jhydrol.2009.08.003, 2009.

591 Hagedorn, F., Schleppe, P., Waldner, P. and Flühler, H.: Export of dissolved organic carbon and
592 nitrogen from Gleysol dominated catchments – the significance of water flow paths,
593 *Biogeochemistry*, 50, 137–161, 2000.

594 Harmon, M. E., Bond-Lamberty, B., Tang, J. and Vargas, R.: Heterotrophic respiration in
595 disturbed forests: A review with examples from North America, *J. Geophys. Res.*
596 *Biogeosciences*, 116(2), 1–17, doi:10.1029/2010JG001495, 2011.

597 Hartmann, A., Barberá, J. A., Lange, J., Andreo, B. and Weiler, M.: Progress in the hydrologic
598 simulation of time variant recharge areas of karst systems – Exemplified at a karst spring in
599 Southern Spain, *Adv. Water Resour.*, 54, 149–160, doi:10.1016/j.advwatres.2013.01.010,

600 2013a.

601 Hartmann, A., Gleeson, T., Rosolem, R., Pianosi, F., Wada, Y. and Wagener, T.: A large-scale
602 simulation model to assess karstic groundwater recharge over Europe and the Mediterranean,
603 *Geosci. Model Dev.*, 8(6), 1729–1746, doi:10.5194/gmd-8-1729-2015, 2015.

604 Hartmann, A., Goldscheider, N., Wagener, T., Lange, J. and Weiler, M.: Karst water resources
605 in a changing world: Review of hydrological modeling approaches, *Rev. Geophys.*, 52(3), 218–
606 242, doi:10.1002/2013rg000443, 2014a.

607 Hartmann, A., Kralik, M., Humer, F., Lange, J. and Weiler, M.: Identification of a karst
608 system's intrinsic hydrodynamic parameters: upscaling from single springs to the whole
609 aquifer, *Environ. Earth Sci.*, 65(8), 2377–2389, doi:10.1007/s12665-011-1033-9, 2012a.

610 Hartmann, A., Lange, J., Weiler, M., Arbel, Y. and Greenbaum, N.: A new approach to model
611 the spatial and temporal variability of recharge to karst aquifers, *Hydrol. Earth Syst. Sci.*, 16(7),
612 2219–2231, doi:10.5194/hess-16-2219-2012, 2012b.

613 Hartmann, A., Mudarra, M., Andreo, B., Marín, A., Wagener, T. and Lange, J.: Modeling
614 spatiotemporal impacts of hydroclimatic extremes on groundwater recharge at a Mediterranean
615 karst aquifer, *Water Resour. Res.*, 50(8), 6507–6521, doi:10.1002/2014WR015685, 2014b.

616 Hartmann, A., Wagener, T., Rimmer, A., Lange, J., Brielmann, H. and Weiler, M.: Testing the
617 realism of model structures to identify karst system processes using water quality and quantity
618 signatures, *Water Resour. Res.*, 49, 3345–3358, doi:10.1002/wrcr.20229, 2013b.

619 Hartmann, A., Weiler, M., Wagener, T., Lange, J., Kralik, M., Humer, F., Mizyed, N., Rimmer,
620 A., Barberá, J. A., Andreo, B., Butscher, C. and Huggenberger, P.: Process-based karst
621 modelling to relate hydrodynamic and hydrochemical characteristics to system properties,
622 *Hydrol. Earth Syst. Sci.*, 17(8), 3305–3321, doi:10.5194/hess-17-3305-2013, 2013c.

623 Heilman, J. L., Litvak, M. E., McInnes, K. J., Kjelgaard, J. F., Kamps, R. H. and Schwinning,
624 S.: Water-storage capacity controls energy partitioning and water use in karst ecosystems on
625 the Edwards Plateau, Texas, *Ecohydrology*, n/a–n/a, doi:10.1002/eco.1327, 2012.

626 Hirabayashi, Y., Mahendran, R., Koirala, S., Konoshima, L., Yamazaki, D., Watanabe, S., Kim,
627 H. and Kanae, S.: Global flood risk under climate change, *Nat. Clim. Chang.*, 3(9), 816–821,
628 doi:10.1038/nclimate1911, 2013.

629 Högberg, M. N. and Högberg, P.: Extramatrical ectomycorrhizal mycelium contributes one-
630 third of microbial biomass and produces, together with associated roots, half the dissolved
631 organic carbon in a forest soil, *New Phytol.*, 154(3), 791–795, doi:10.1046/j.1469-
632 8137.2002.00417.x, 2002.

633 Huber, C.: Long lasting nitrate leaching after bark beetle attack in the highlands of the Bavarian
634 Forest National Park., *J. Environ. Qual.*, 34(5), 1772–9, doi:10.2134/jeq2004.0210, 2005.

635 Huber, C., Baumgarten, M., Göttlein, A. and Rotter, V.: Nitrogen turnover and nitrate leaching

636 after bark beetle attack in mountainous spruce stands of the Bavarian Forest National Park,
637 Water, Air, Soil Pollut. Focus, 4(2-3), 391–414, doi:10.1023/B:WAFO.0000028367.69158.8d,
638 2004.

639 Humer, F. and Kralik, M.: Integrated Monitoring Zöbelboden: Hydrologische und
640 hydrochemische Untersuchungen, Unpubl. Rep. Environ. Agency, Vienna, 34, 2008.

641 Johnson, M. S., Billett, M. F., Dinsmore, K. J., Wallin, M., Dyson, K. E. and Jassal, R. S.:
642 Direct and continuous measurement of dissolved carbon dioxide in freshwater aquatic systems
643 — method and applications, , 159(August 2011), 145–159, doi:10.1002/eco, 2010.

644 Jost, G., Dirnböck, T., Grabner, M.-T. and Mirtl, M.: Nitrogen Leaching of Two Forest
645 Ecosystems in a Karst Watershed, Water, Air, & Soil Pollut., 218(1-4), 633–649,
646 doi:10.1007/s11270-010-0674-8, 2010.

647 Jourde, H., Mazzilli, N., Lecoq, N., Arfib, B. and Bertin, D.: KARSTMOD: A Generic Modular
648 Reservoir Model Dedicated to Spring Discharge Modeling and Hydrodynamic Analysis in
649 Karst, in Hydrogeological and Environmental Investigations in Karst Systems SE - 38, vol. 1,
650 edited by B. Andreo, F. Carrasco, J. J. Durán, P. Jiménez, and J. W. LaMoreaux, pp. 339–344,
651 Springer Berlin Heidelberg., 2015.

652 Kaiser, K. and Kalbitz, K.: Cycling downwards - dissolved organic matter in soils, Soil Biol.
653 Biochem., 52, 29–32, doi:10.1016/j.soilbio.2012.04.002, 2012.

654 Kalbitz, K., Meyer, A., Yang, R. and Gerstberger, P.: Response of dissolved organic matter in
655 the forest floor to long-term manipulation of litter and throughfall inputs, Biogeochemistry,
656 86(3), 301–318, doi:10.1007/s10533-007-9161-8, 2007.

657 Katz, B. G., Böhlke, J. K. and Hornsby, H. D.: Timescales for nitrate contamination of spring
658 waters, northern Florida, USA, Chem. Geol., 179(1-4), 167–186, 2001.

659 Katz, B. G., Chelette, A. R. and Pratt, T. R.: Use of chemical and isotopic tracers to assess
660 nitrate contamination and ground-water age, Woodville Karst Plain, USA, J. Hydrol., 289(1-
661 4), 36–61, doi:10.1016/j.jhydrol.2003.11.001, 2004.

662 Katzensteiner, K.: Effects of harvesting on nutrient leaching in a Norway spruce (*Picea*, Plant
663 Soil, 250, 59–73, 2003.

664 Kiese, R., Heinzeller, C., Werner, C., Wochele, S., Grote, R. and Butterbach-Bahl, K.:
665 Quantification of nitrate leaching from German forest ecosystems by use of a process oriented
666 biogeochemical model., Environ. Pollut., 159(11), 3204–14,
667 doi:10.1016/j.envpol.2011.05.004, 2011.

668 Klemeš, V.: Dilettantism in Hydrology: Transition or Destiny, Water Resour. Res., 22(9),
669 177S–188S, 1986.

670 Kobler, J., Jandl, R., Dirnböck, T., Mirtl, M. and Schindlbacher, A.: Effects of stand patchiness
671 due to windthrow and bark beetle abatement measures on soil CO₂ efflux and net ecosystem

- 672 productivity of a managed temperate mountain forest, *Eur. J. For. Res.*, 13, 683–692,
673 doi:10.1007/s10342-015-0882-2, 2015.
- 674 Kordilla, J., Sauter, M., Reimann, T. and Geyer, T.: Simulation of saturated and unsaturated
675 flow in karst systems at catchment scale using a double continuum approach, *Hydrol. Earth*
676 *Syst. Sci.*, 16(10), 3909–3923, doi:10.5194/hess-16-3909-2012, 2012.
- 677 Kralik, M., Humer, F., Grath, J., Numi-Legat, J., Hanus-Illnar, A., Halas, S. and Jelenc, M.:
678 Impact of long distance air pollution on sensitive karst groundwater resources estimated by
679 means of Pb-, S-, O- and Sr-isotopes, in *Karst, cambio climático y aguas subterráneas*, edited
680 by J. J. Duran, B. Andreo, and F. Carrasco, pp. 311–317, *Publicaciones del Instituto Geológico*
681 *y Minero de España, Serie: Hydrogeología y Aguas Subterráneas N.º 18*, Madrid., 2006.
- 682 Kralik, M., Humer, F., Papesch, W., Tesch, R., Suckow, A., Han, L. F. and Groening, M.:
683 Karstwater-ages in an alpine dolomite catchment , Austria : ^{18}O , ^3H , $^3\text{H} / ^3\text{He}$, CFC and dye
684 tracer investigations, *Geophys. Res. Abstr.*, 11, 11403, European Geosciences Union, General
685 Assembl, 2009.
- 686 Lindroos, A. J., Derome, J., Mustajärvi, K., Nöjd, P., Beuker, E. and Helmisaari, H. S.: Fluxes
687 of dissolved organic carbon in stand throughfall and percolation water in 12 boreal coniferous
688 stands on mineral soils in Finland, *Boreal Environ. Res.*, 13(SUPPL. B), 22–34, 2008.
- 689 Löfgren, S., Fröberg, M., Yu, J., Nisell, J. and Ranney, B.: Water chemistry in 179 randomly
690 selected Swedish headwater streams related to forest production, clear-felling and climate,
691 *Environ. Monit. Assess.*, 186(12), 8907–8928, doi:10.1007/s10661-014-4054-5, 2014.
- 692 Mahler, B. J. and Garner, B. D.: Using Nitrate to Quantify Quick Flow in a Karst Aquifer,
693 *Ground Water*, 47(3), 350–360 [online] Available from: [http://dx.doi.org/10.1111/j.1745-](http://dx.doi.org/10.1111/j.1745-6584.2008.00499.x)
694 [6584.2008.00499.x](http://dx.doi.org/10.1111/j.1745-6584.2008.00499.x), 2009.
- 695 Meyer, J. L., Tate, C. M. and Feb, N.: The Effects of Watershed Disturbance on Dissolved
696 Organic Carbon Dynamics of a Stream T H E E F F E C T S O F WATERSHED
697 DISTURBANCE ON DISSOLVED, , 64(1), 33–44, 1983.
- 698 Michalzik, B., Kalbitz, K., Park, J., Solinger, S. and Matzner, E.: Fluxes and concentrations of
699 dissolved organic carbon and nitrogen—a synthesis for temperate forests, *Biogeochemistry*, 52,
700 173–205 [online] Available from: <http://link.springer.com/article/10.1023/A:1006441620810>,
701 2001.
- 702 Mikkelsen, K. M., Bearup, L. a., Maxwell, R. M., Stednick, J. D., McCray, J. E. and Sharp, J.
703 O.: Bark beetle infestation impacts on nutrient cycling, water quality and interdependent
704 hydrological effects, *Biogeochemistry*, 115, 1–21, doi:10.1007/s10533-013-9875-8, 2013.
- 705 Le Moine, N., Andréassian, V. and Mathevet, T.: Confronting surface- and groundwater
706 balances on the La Rochefoucauld-Touvre karstic system (Charente, France), *Water Resour.*
707 *Res.*, 44, W03403, doi:10.1029/2007WR005984, 2008.

708 Monteith, S. S., Buttle, J. M., Hazlett, P. W., Beall, F. D., Semkin, R. G. and Jeffries, D. S.:
709 Paired-basin comparison of hydrologic response in harvested and undisturbed hardwood forests
710 during snowmelt in central Ontario: II. Streamflow sources and groundwater residence times,
711 *Hydrol. Process.*, 20(5), 1117–1136, doi:10.1002/hyp.6073, 2006.

712 Neff, J. C. and Asner, G. P.: Dissolved organic carbon in terrestrial ecosystems: Synthesis and
713 a model, *Ecosystems*, 4(1), 29–48, doi:10.1007/s100210000058, 2001.

714 Perrin, J., Jeannin, P.-Y. and Zwahlen, F.: Epikarst storage in a karst aquifer: a conceptual
715 model based on isotopic data, Milandre test site, Switzerland, *J. Hydrol.*, 279, 106–124, 2003.

716 Pinault, J.-L., Pauwels, H. and Cann, C.: Inverse modeling of the hydrological and the
717 hydrochemical behavior of hydrosystems: Application to nitrate transport and denitrification,
718 *Water Resour. Res.*, 37(8), 2179–2190, 2001.

719 Raymond, P. a. and Saiers, J. E.: Event controlled DOC export from forested watersheds,
720 *Biogeochemistry*, 100(1-3), 197–209, doi:10.1007/s10533-010-9416-7, 2010.

721 Rimmer, A. and Salinger, Y.: Modelling precipitation-streamflow processes in karst basin: The
722 case of the Jordan River sources, Israel, *J. Hydrol.*, 331, 524–542, 2006.

723 Rogora, M., Mosello, R., Arisci, S., Brizzio, M. C., Barbieri, a., Balestrini, R., Waldner, P.,
724 Schmitt, M., Stähli, M., Thimonier, a., Kalina, M., Puxbaum, H., Nickus, U., Ulrich, E. and
725 Probst, a.: An Overview of Atmospheric Deposition Chemistry over the Alps: Present Status
726 and Long-term Trends, *Hydrobiologia*, 562(1), 17–40, doi:10.1007/s10750-005-1803-z, 2006.

727 Sakamoto, T., Takahashi, M., Terajima, T., Nakai, Y. and Matsuura, Y.: Comparison of the
728 effects of rainfall and snowmelt on the carbon discharge of a small, steep, forested watershed
729 in Hokkaido, northern Japan., *Hydrol. Process.*, 13(May 1998), 2301–2314,
730 doi:10.1002/(SICI)1099-1085(199910)13:14/15<2301::AID-HYP876>3.0.CO;2-U, 1999.

731 Sanderman, J., Lohse, K. a., Baldock, J. a. and Amundson, R.: Linking soils and streams:
732 Sources and chemistry of dissolved organic matter in a small coastal watershed, *Water Resour.*
733 *Res.*, 45(3), 1–13, doi:10.1029/2008WR006977, 2009.

734 Seidl, R., Schelhaas, M., Rammer, W. and Verkerk, P. J.: Increasing forest disturbances in
735 Europe and their impact on carbon storage, *Nat. Clim. Chang.*, 4(September), 1–6,
736 doi:10.1038/nclimate2318, 2014.

737 Solinger, S., Kalbitz, K. and Matzner, E.: Controls on the dynamics of dissolved organic carbon
738 and nitrogen in a Central European deciduous forest, *Biogeochem*, 55, 327–349, 2001.

739 Terajima, T. and Moriizumi, M.: Temporal and spatial changes in dissolved organic carbon
740 concentration and fluorescence intensity of fulvic acid like materials in mountainous headwater
741 catchments, *J. Hydrol.*, 479, 1–12, doi:10.1016/j.jhydrol.2012.10.023, 2013.

742 Tissier, G., Perrette, Y., Dzikowski, M., Poulenard, J., Hobléa, F., Malet, E. and Fanget, B.:
743 Seasonal changes of organic matter quality and quantity at the outlet of a forested karst system

744 (La Roche Saint Alban, French Alps), *J. Hydrol.*, 482, 139–148,
745 doi:10.1016/j.jhydrol.2012.12.045, 2013.

746 Tritz, S., Guinot, V. and Jourde, H.: Modelling the behaviour of a karst system catchment using
747 non-linear hysteretic conceptual model, *J. Hydrol.*, 397(3-4), 250–262,
748 doi:10.1016/j.jhydrol.2010.12.001, 2011.

749 Verstraeten, A., De Vos, B., Neiryneck, J., Roskams, P. and Hens, M.: Impact of air-borne or
750 canopy-derived dissolved organic carbon (DOC) on forest soil solution DOC in Flanders,
751 Belgium, *Atmos. Environ.*, 83, 155–165, doi:10.1016/j.atmosenv.2013.10.058, 2014.

752 Vrugt, J. A., Gupta, H. V, Bouten, W. and Sorooshian, S.: A Shuffled Complex Evolution
753 Metropolis algorithm for optimization and uncertainty assessment of hydrologic model
754 parameters, *Water Resour. Res.*, 39(8), 1201, doi:10.1029/2002WR001642, 2003.

755 Vrugt, J. A., Gupta, H. V, Dekker, S. C., Sorooshian, S., Wagener, T. and Bouten, W.:
756 Application of stochastic parameter optimization to the Sacramento Soil Moisture Accounting
757 model, *J. Hydrol.*, 325(1-4), 288–307, doi:10.1016/j.jhydrol.2005.10.041, 2006.

758 Weis, W., Rotter, V. and Göttlein, A.: Water and element fluxes during the regeneration of
759 Norway spruce with European beech: Effects of shelterwood-cut and clear-cut, *For. Ecol.
760 Manage.*, 224(3), 304–317, doi:10.1016/j.foreco.2005.12.040, 2006.

761 Weishaar, J. L., Aiken, G. R., Bergamaschi, B. A., Fram, M. S., Fujii, R. and Mopper, K.:
762 Evaluation of Specific Ultraviolet Absorbance as an Indicator of the Chemical Composition
763 and Reactivity of Dissolved Organic Carbon, *Environ. Sci. Technol.*, 37(20), 4702–4708,
764 doi:10.1021/es030360x, 2003.

765 WRB: World reference base for soil resources, edited by FAO, IUSS Working Group, Rome.
766 [online] Available from: <http://www.fao.org/ag/agl/agll/wrb/doc/wrb2006final.pdf>, 2006.

767 Wu, H., Peng, C., Moore, T. R., Hua, D., Li, C., Zhu, Q., Peichl, M., Arain, M. a. and Guo, Z.:
768 Modeling dissolved organic carbon in temperate forest soils: TRIPLEX-DOC model
769 development and validation, *Geosci. Model Dev.*, 7(3), 867–881, doi:10.5194/gmd-7-867-
770 2014, 2014.

771 Wu, Y., Clarke, N. and Mulder, J.: Dissolved Organic Nitrogen Concentrations and Ratios of
772 Dissolved Organic Carbon to Dissolved Organic Nitrogen in Throughfall and Soil Waters in
773 Norway Spruce and Scots Pine Forest Stands Throughout Norway, *Water, Air, Soil Pollut.*,
774 210(1-4), 171–186, doi:10.1007/s11270-009-0239-x, 2009.

775

776

777 **10 Table captions**

778 Table 1: model parameters, description, ranges and calibrated values with *KGE* performances
779 for the calibration and validation samples

780 Table 2: calibrated pre-storm parameters for DIN dynamics and 2 scenarios for adapting it at the
781 stormy period

782 **11 Figure captions**

783 Figure 1: study site and location of measurement devices (Hartmann et al., 2012a;modified).

784 Figure 2: Intra-annual and inter-annual variations of (a) DOC concentrations, (c) DIN
785 concentrations and (e) discharge, and relation between discharge and (b) DOC and (d) DIN
786 before and during the wind disturbance period.

787 Figure 3: Sketch of model structure; it is assumed that discharge and hydrochemistry at the two
788 weirs is composed by different mixtures of diffuse recharge (green), concentrated recharge
789 (red), diffuse groundwater flow (blue) and concentrated groundwater flow (purple)

790 Figure 4: Observed versus simulated discharges for the entire karst system and weir 1
791 Observed versus simulated discharges for the entire karst system and weir 1
792 Figure 5: Observed versus simulated (a) DOC and (b) DIN at weir 1.

793 Figure 5: Observed versus simulated (a) DOC and (b) DIN at weir 1.

794 Figure 6: Individual components of the *KGE*: (a) ratio of simulated and observed variabilities,
795 (b) ratio of simulated and observed average values, and (c) their correlation for the wind
796 disturbance period; for comparison the *KGE* components and their inter-annual variability are
797 also shown for pre-storm period and after the correction of the DIN production model
798 parameters during the wind period.

799 Figure 7: Observed and simulated DIN dynamics using the pre-storm parameters (red line), the
800 scenario 1 parameters derived from the deviations assessed by the *KGE* components (orange
801 line), and the scenario 2 parameters derived by systematic variation (dark red line).

802 Figure 8: Mean transit times for (a) the soil and epikarst and (c) the groundwater storages
803 derived by an infinite virtual tracer injection starting with the beginning of the wind disturbance
804 period, and the reaction of (b) the soil and epikarst, and (d) the groundwater storage as the
805 impact ends.

806 **12 Tables**807 **Table 1: model parameters, description, ranges and calibrated values with *KGE* performances for the**
808 **calibration and validation samples**

Parameter	Description	Unit	Ranges		Optimized values	
			Lower	Upper	Sample 1	Sample 2
$V_{mean,S}$	Mean soil storage capacity	mm	0	1500	450.18	599.13
$f_{var,S}$	fraction of the spoil that has a variable depth	-	0	1	0.06	0.02
$V_{mean,E}$	Mean epikarst storage capacity	mm	0	1500	1495.49	1233.98
a_{SE}	Soil/epikarst depth variability constant	-	0	2	1.69	1.91
$K_{mean,E}$	Epikarst mean storage constant	d	1	50	2.65	8.27
a_{fsep}	Recharge separation variability constant	-	0	2	0.88	1.44
K_C	Conduit storage constant	d	1	10	1.37	1.03
a_{GW}	Groundwater variability constant	-	0	2	2.00	1.88
f_{EW}	Fraction of weir discharge originating from the epikarst	-	0	1	0.56	0.72
$f_{WE,conc}$	Fraction of weir discharge originating from the epikarst as concentrated flow	-	0	1	0.57	0.47
$f_{WGW,conc}$	fraction of weir discharge originating from the groundwater as concentrated flow	-	0	1	0.01	0.06
P_{DOC}	DOC production parameter	mg l ⁻¹	0	15	1.79	1.57
a_{DOC}	DOC variability constant	-	0	2	0.92	1.05
P_{DIN}	DIN production parameter	mg l ⁻¹	-5	10	-1.35	0.11
$S_{PH,DIN}$	Phase of annual DIN production	d	0	365	0	2
A_{DIN}	Amplitude of annual DIN production	mg l ⁻¹	0	10	3.36	1.84
$G_{max,SO4}$	Equilibrium concentration of SO ₄ in matrix	mg l ⁻¹	0	50	2.74	3.07
a_{Geo}	Equilibrium concentration variability constant	-	0	2	0.11	0.04
$KGE_{weighted}$	weighted multi-objective model performance	-	0	1	0.56/0.49*	0.52/0.53*
$KGE_{Q,tot}$	model performance for discharge of entire system	-	0	1	0.41/0.33*	0.35/0.42*
$KGE_{Q,W}$	model performance for discharge of weir	-	0	1	0.67/0.62*	0.61/0.66*
KGE_{DOC}	model performance for DOC concentrations	-	0	1	0.38/0.35*	0.43/0.32*
KGE_{DIN}	model performance for NO ₃ concentrations	-	0	1	0.48/0.40*	0.48/0.45*
KGE_{SO4}	model performance for SO ₄ concentrations	-	0	1	0.74/0.62*	0.64/0.65*

809 * calibration/validation with other sample

810

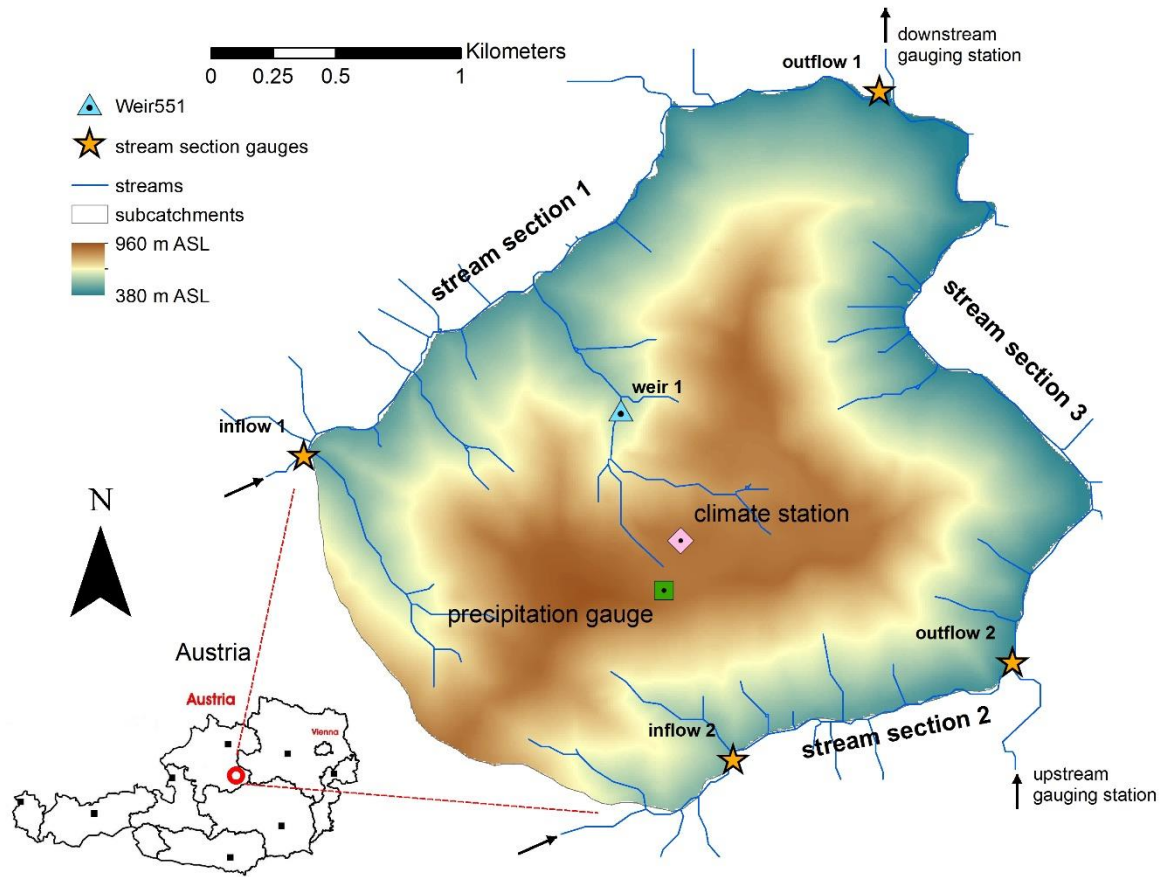
811 **Table 2: calibrated pre-storm parameters for DIN dynamics and 2 scenrios for adapting it at the stormy**
812 **period**

Parameter	Unit	Calibration type		
		Pre-storm	manual	automatic
P_{DIN}	mg l ⁻¹	0.11	2.10	0.00
$S_{PH,DIN}$	d	2.00	9.00	23
A_{DIN}	mg l ⁻¹	1.80	0.70	2.63
KGE_{DIN}^*	-	0.29	0.41	0.46
variability α_{DIN}^*	-	0.75	1.04	1.05
bias β_{DIN}^*	-	0.70	1.01	0.83
correlation $_{DIN}^*$	-	0.40	0.41	0.49

* for 2006/07-2011/12

813

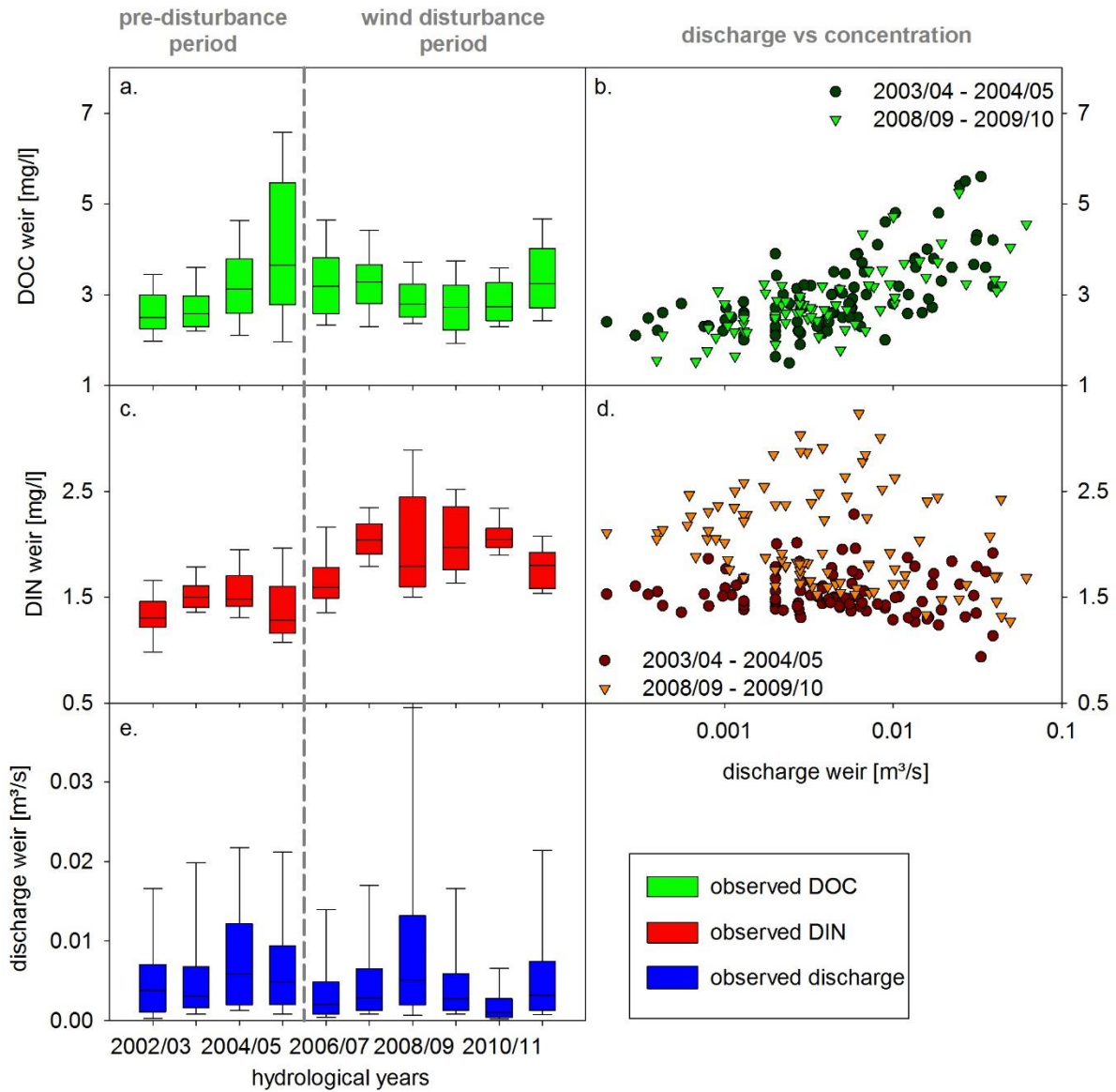
814 **13 Figures**



815

816 **Figure 1: study site and location of measurement devices (Hartmann et al., 2012a;modified).**

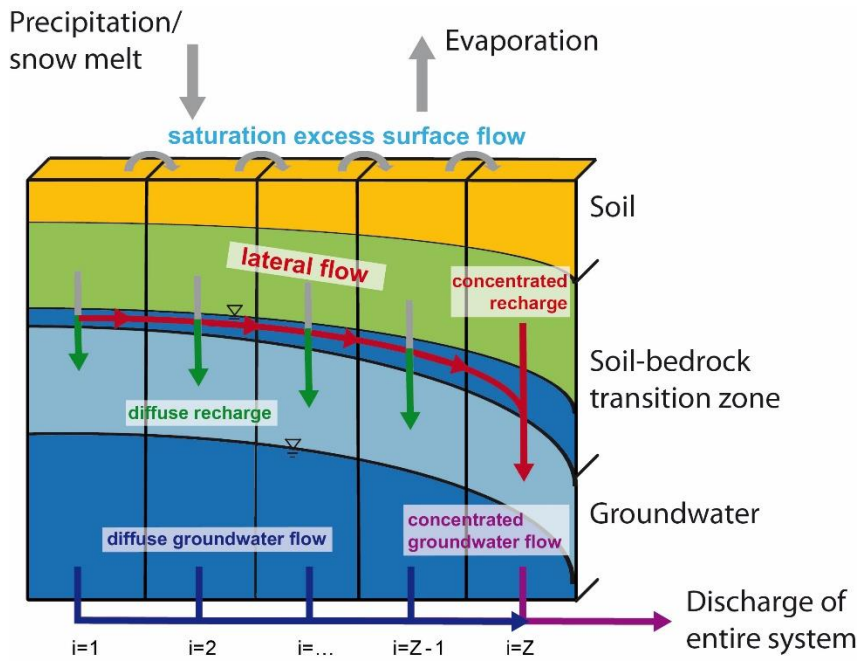
817



818

819 **Figure 2: Intra-annual and inter-annual variations of (a) DOC concentrations, (c) DIN concentrations and**
 820 **(e) discharge, and relation between discharge and (b) DOC and (d) DIN before and during the wind**
 821 **disturbance period.**

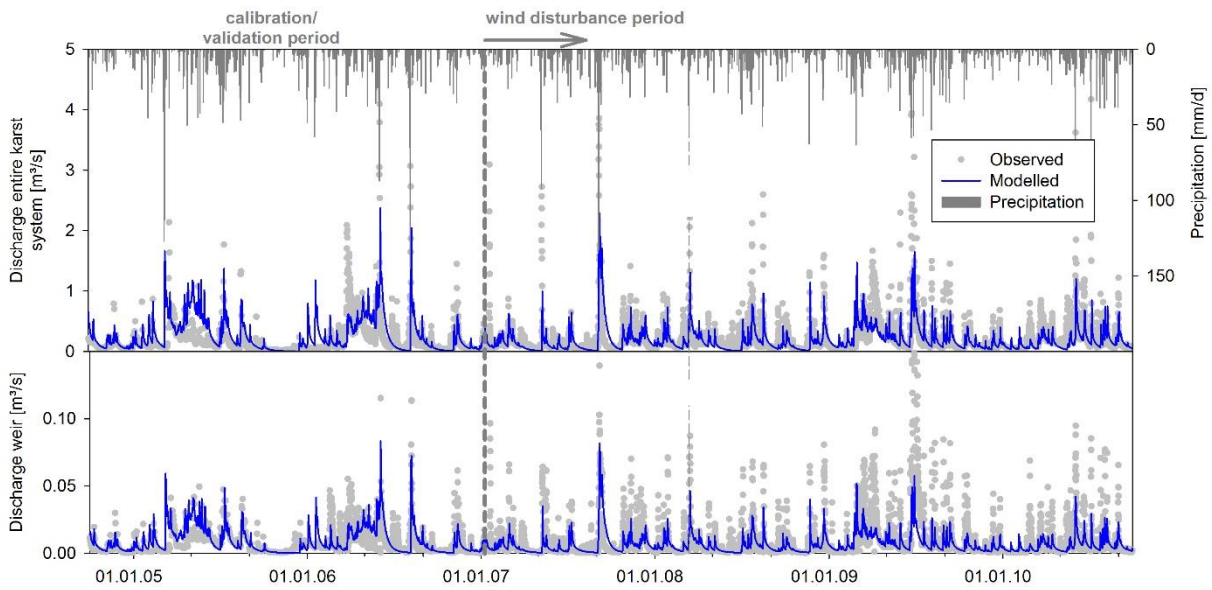
822



823

824 **Figure 3: Sketch of model structure; it is assumed that discharge and hydrochemistry at the two weirs is**
 825 **composed by different mixtures of diffuse recharge (green), concentrated recharge (red), diffuse**
 826 **groundwater flow (blue) and concentrated groundwater flow (purple)**

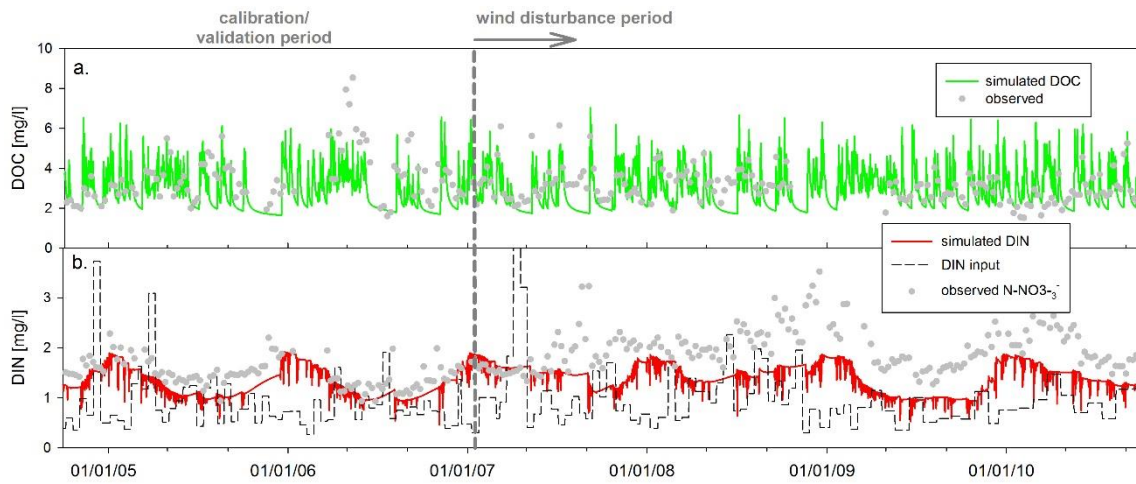
827



828

829 **Figure 4: Observed versus simulated discharges for the entire karst system and weir 1**

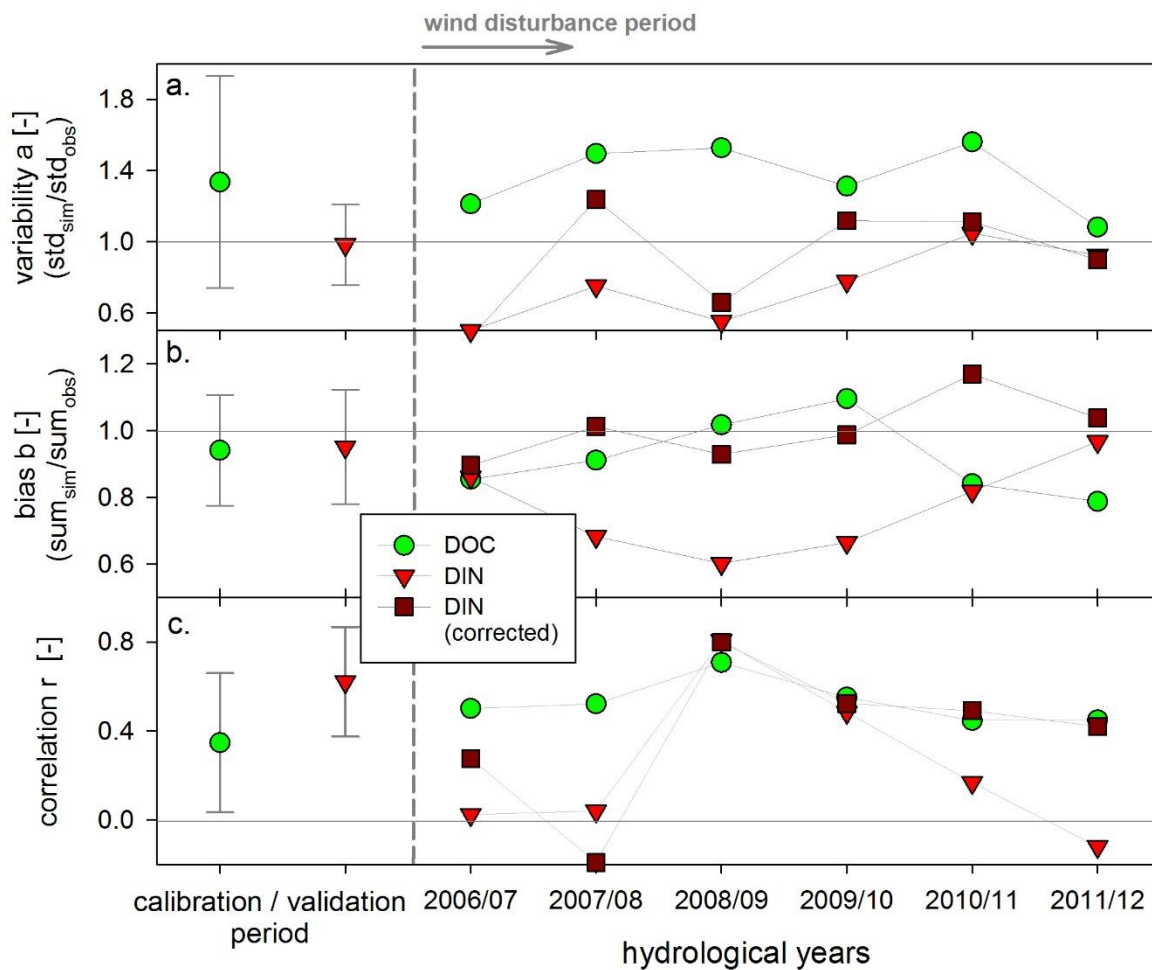
830



831

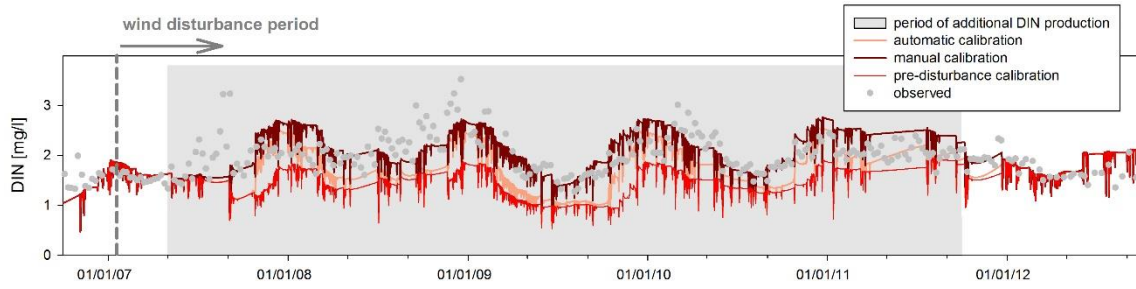
832 **Figure 5: Observed versus simulated (a) DOC and (b) DIN at weir 1.**

833



834

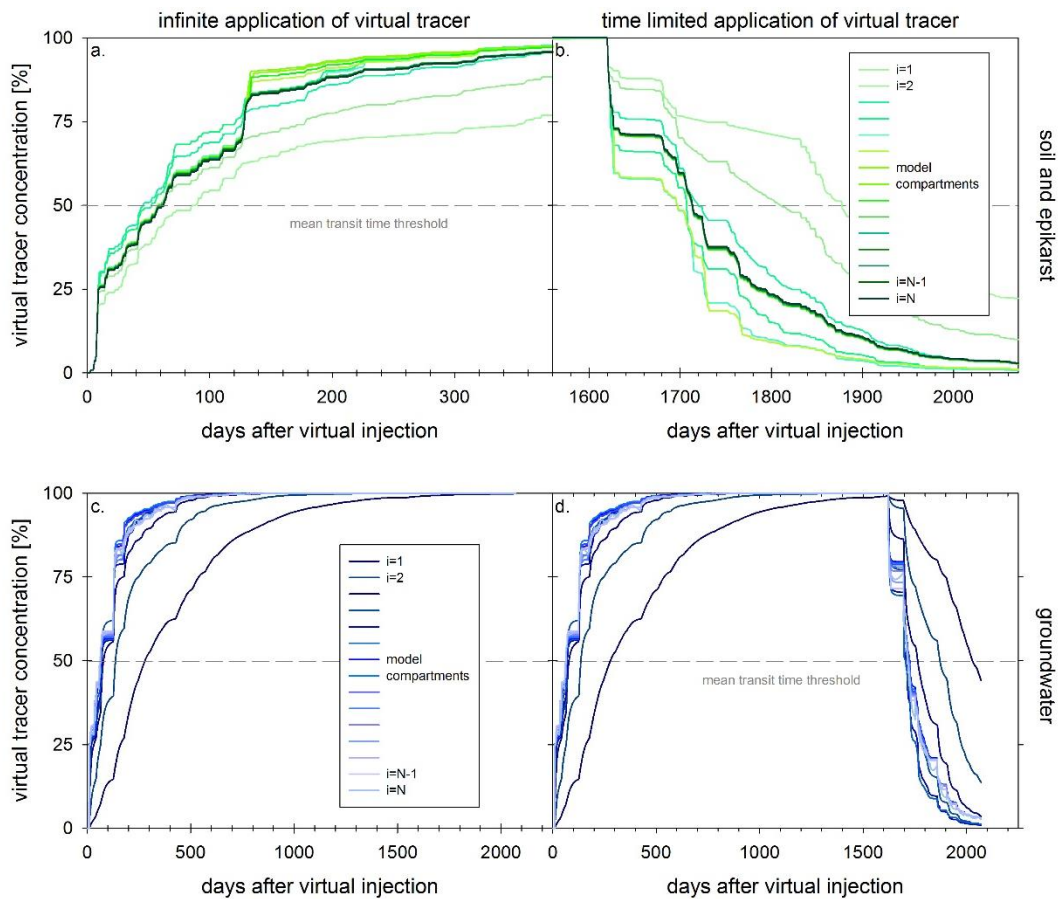
835 **Figure 6: Individual components of the KGE: (a) ratio of simulated and observed variabilities, (b) ratio of**
 836 **simulated and observed average values, and (c) their correlation for the wind disturbance period; for**
 837 **comparison the KGE components and their inter-annual variability are also shown for pre-storm period**
 838 **and after the correction of the DIN production model parameters during the wind period.**



840

841 **Figure 7: Observed and simulated DIN dynamics using the pre-storm parameters (red line), the scenario 1**
 842 **parameters derived from the deviations assessed by the KGE components (orange line), and the scenario 2**
 843 **parameters derived by systematic variation (dark red line).**

844



845

846 **Figure 8: Mean transit times for (a) the soil and epikarst and (c) the groundwater storages derived by an**
 847 **infinite virtual tracer injection starting with the beginning of the wind disturbance period, and the reaction**
 848 **of (b) the soil and epikarst, and (d) the groundwater storage as the impact ends.**